

Simulation of aggregating particles in complex flows by the lattice kinetic Monte Carlo method

Matthew H. Flamm, Talid Sinno,^{a)} and Scott L. Diamond^{b)}

Department of Chemical and Biomolecular Engineering, University of Pennsylvania, Philadelphia, Pennsylvania 19104, USA

(Received 8 July 2010; accepted 8 November 2010; published online 21 January 2011)

We develop and validate an efficient lattice kinetic Monte Carlo (LKMC) method for simulating particle aggregation in laminar flows with spatially varying shear rate, such as parabolic flow or flows with standing vortices. A contact time model was developed to describe the particle-particle collision efficiency as a function of the local shear rate, G , and approach angle, θ . This model effectively accounts for the hydrodynamic interactions between approaching particles, which is not explicitly considered in the LKMC framework. For imperfect collisions, the derived collision efficiency [$\varepsilon = 1 - \int_0^{\pi/2} \sin \theta \exp(-2 \cot \theta \Gamma_{\text{agg}}/G) d\theta$] was found to depend only on Γ_{agg}/G , where Γ_{agg} is the specified aggregation rate. For aggregating platelets in tube flow, $\Gamma_{\text{agg}} = 0.683 \text{ s}^{-1}$ predicts the experimentally measured ε across a physiological range ($G = 40\text{--}1000 \text{ s}^{-1}$) and is consistent with $\alpha_{2b}\beta_3$ -fibrinogen bond dynamics. Aggregation in parabolic flow resulted in the largest aggregates forming near the wall where shear rate and residence time were maximal, however intermediate regions between the wall and the center exhibited the highest aggregation rate due to depletion of reactants nearest the wall. Then, motivated by stenotic or valvular flows, we employed the LKMC simulation developed here for baffled geometries that exhibit regions of squeezing flow and standing recirculation zones. In these calculations, the largest aggregates were formed within the vortices (maximal residence time), while squeezing flow regions corresponded to zones of highest aggregation rate. © 2011 American Institute of Physics. [doi:10.1063/1.3521395]

I. INTRODUCTION

A large class of problems is defined broadly by the processes of particulate aggregation and fragmentation in the presence of fluid flow. Particles moving within a shearing fluid have spatially varying velocities that control the dynamics of particle collisions [Fig. 1(a)]. Examples include cluster growth of paramagnetic particles in microchannels,¹ aerosol pollutant aggregation within the atmosphere,² and cell aggregation in blood flow.^{3–5} Much work has focused on mean-field approaches, i.e., the solution of the population balance (or Smoluchowski) equations.⁶ In the classical population balance equation (PBE) approach, the particle size distribution is found by solving continuum-scale differential equations, in which the aggregation and fragmentation kernels that describe particle-particle interactions are usually derived from a combination of kinetic theory, hydrodynamics, and problem-specific chemical, biological, or physical sources of interactions. However, mean-field representations of particle aggregation driven by convection are limited to relatively simple cases. While the influence of hydrodynamic and particle-particle interactions has been studied extensively for constant shear rate,^{7,8} PBE approaches do not address many common and realistic situations including tube flow. A direct simulation method is needed for modeling processes with complex flow fields.

At the other end of the computational spectrum are methods that fully resolve the coupling between the particles themselves and between the particles and the fluid. One example is the direct numerical simulation of the momentum equations in which multiple rigid or elastically deformable particles are present.⁹ Recently, lattice Boltzmann and dissipative particle dynamics also have been employed for this purpose.^{10,11} While these direct approaches fully resolve the flow at the particle scale and thus capture accurately the hydrodynamic interactions between particles, they are computationally expensive for that same reason. As a result, a slew of coarse-grained approaches have emerged that allow explicit aggregate morphology to be retained while removing the full coupling between individual particles and the fluid. Marshall used a discrete-element model for soft attractive particles with a prescribed velocity profile to simulate hundreds to thousands of particles in two-dimensional (2D) parabolic flow¹² and micronozzle flow.¹³ In the context of cellular deposition problems, Leiderman and Fogelson developed a spatially resolved continuum model for platelet aggregation to an injured blood vessel wall that includes coupling between the flow and the growing platelet deposit.¹⁴ Xu *et al.* used a cellular Potts model to simulate deformable platelet adhesion to an injured blood vessel wall that also couples the fluid flow to the growing platelet aggregate.^{15,16}

In the present work, a new coarse-grained approach based on the lattice kinetic Monte Carlo (LKMC) method is presented for describing the general physics of particle aggregation in a prescribed, nonuniform flow field. LKMC

^{a)}Electronic mail: talid@seas.upenn.edu.

^{b)}Electronic mail: sld@seas.upenn.edu.

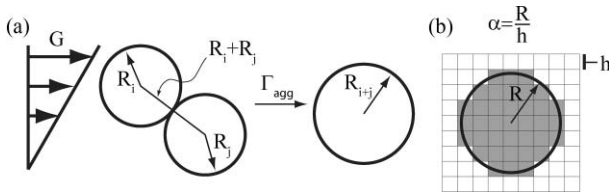


FIG. 1. Aggregation events on a lattice. (a) Colliding particles undergo an aggregation event with constant rate Γ_{agg} to form a new particle with radius $R_{i+j} = \sqrt{R_i^2 + R_j^2}$. The collision radius between the colliding particles i and j is given by $R_i + R_j$. (b) Particles are discretized on the lattice with lattice spacing h . The resolution of the particle radius on the lattice is given by α .

is well-suited for studying nonequilibrium aggregation processes and has been applied to bulk crystal growth,¹⁷ epitaxial deposition,¹⁸ microstructure evolution,^{19,20} and numerous other applications. One particularly appealing aspect of LKMC is the possibility for coarse-graining.^{21,22} A common feature in these examples of LKMC modeling is the absence of convective transport whereby all particle motion is purely diffusive. Recently, Flamm *et al.*²³ reported an LKMC algorithm for including convective particle transport in a prescribed flow field. In Ref. 23, particles were considered to be noninteracting tracers that did not influence the flow and only interacted with each other through a no-overlap (excluded volume) interaction. The LKMC approach was demonstrated to be efficient and accurate when compared to numerical solution of idealized convection-diffusion problems (no aggregation). Here, this method is extended to include explicit particle aggregation, while retaining the advantages of the LKMC approach.

II. THE LATTICE KINETIC MONTE CARLO ALGORITHM

The inputs for an LKMC simulation are the rates for all possible events in the system at a given configuration. In the present case, events consist of particle motion (by convection or diffusion) and particle aggregation. The discretization of the system onto a lattice reduces the degrees of freedom in the system and makes possible the tabulation of all possible events at a given configuration. For all simulations reported here, we employ a two-dimensional, uniform square lattice with spacing h , although we note that all aspects of the model can be extended to three dimensions. At any given time, each particle can move one lattice space in either lattice direction for a total of four possible moves per particle in two dimensions. We introduce a grid resolution parameter, $\alpha = R/h$ [Fig. 1(b)], where R is the radius of a particle. For all simulations, the reported value of α corresponds to the resolution of the monomers on the lattice ($\alpha = R_0/h$).

As shown previously in Ref. 23, the rate Γ for a convective move across one lattice space along a principal lattice direction (i.e., e_x or e_y) is given by

$$\Gamma_C = \frac{v}{h}, \quad (1)$$

where $v = v(x, y)$ is the magnitude of the local fluid velocity in that direction. The velocity for a particle is given by the average velocity over all particle-occupied lattice sites. The

rate for a diffusive move of one lattice space in either of the principal lattice directions is

$$\Gamma_D = \frac{D}{h^2}, \quad (2)$$

where D is the diffusion coefficient of the particle. The simplest method to combine convective and diffusive moves is to add rates in the directions of positive flow velocity, i.e.,

$$\Gamma = \Gamma_C + \Gamma_D, \quad (3)$$

while only the diffusive component is applied in directions of zero or negative flow velocity. In this work, we only consider cases driven by convective motion ($D = 0$). During a move event, the particle (or aggregate) is moved by one lattice space in the direction chosen by the LKMC algorithm. After the move is executed, the rates associated with the moving particle and its immediate neighbors are updated, while all other rates are unchanged. Site exclusion is enforced by setting the rate of events causing overlap to 0.

Direct incorporation of convective transport into an LKMC simulation as described above generates nonphysical particle motion due to concentration-dependent particle blocking induced by the sequential move nature of the LKMC algorithm. In Ref. 23, this artifact was removed using a pass-forward algorithm (PFA) in which particles at the front of connected chains were assigned the convective contributions of the blocked particles. By reintroducing the blocked convective rates by passing forward these rates to the first available particle in the direction of flow, the correct concentration-independent velocity was obtained. Although the PFA was shown to remove the systematic bias of particle blocking, the LKMC simulation of convection intrinsically introduces an algorithmic diffusive error into the dynamics that scales as²³

$$D_{err} = \frac{vh}{2} \quad (4)$$

in the limit of zero concentration; this additional diffusion arises from the randomness in particle selection as well as the stochastic nature of clock update in the LKMC method. Recall that v is the velocity magnitude along a particular lattice direction, so that D_{err} is anisotropic if $v_x \neq v_y$ and, in general, spatially varying for an arbitrary velocity field. The algorithmic diffusive error in the limit of pure convection can be parametrized in terms of an error Peclet number, i.e.,

$$Pe_{LKMC} = \frac{vR}{D_{err}} = \frac{vR}{vh/2} = 2\alpha. \quad (5)$$

Thus, for a purely convective situation (i.e., insignificant Brownian motion), Pe_{LKMC} remains finite because of algorithm diffusion, but can be increased arbitrarily by increasing α , i.e., increasing the grid resolution relative to a monomer radius. Increasing lattice resolution, α , increases the number of moves required for a particle or aggregate to traverse a given distance, thereby increasing the computational cost of the simulation. Note, however, that the number of possible particle events at any given time is unchanged. It should also be noted that as the particle size distribution coarsens during

a simulation, the effective value of Pe_{LKMC} actually increases, i.e., the relative importance of artificial diffusion will be reduced.

In addition to particle moves, an aggregation event can occur when two particles become adjacent to one another. Aggregation occurs with a prescribed rate, Γ_{agg} , which is another input into the LKMC model. In the present work, when an aggregation event is executed, immediate morphological relaxation is performed so that our results can be compared to PBE predictions. For an aggregation event between two particles of size R_i and R_j , a new particle of size $\sqrt{R_i^2 + R_j^2}$ is placed at the nearest lattice site to the center of mass of the original particles. This choice of particle size conserves total particle area (or mass). If the new particle overlaps another particle on the lattice, the new particle is placed at the nearest position that has no overlap. Other types of aggregate morphological relaxation dynamics can be included into the LKMC framework by modeling the relaxation process explicitly; the idealized choice used in the following calculations simplifies the comparison to PBE model predictions. In the limit of perfect, or ideal, collisions ($\Gamma_{agg} = \infty$), once the particles come into contact, they immediately aggregate. In practice, we set Γ_{agg} to a value that is several orders of magnitude larger than the next largest rate in the system to simulate perfect collision efficiency. For finite values of Γ_{agg} , the probability that an aggregation event occurs after particle contact is given by the collision efficiency, ε . A model for imperfect, or nonideal, collisions that establishes a connection between a given value of ε and the corresponding Γ_{agg} is described later in Sec. III B.

The remainder of the LKMC algorithm proceeds in a similar fashion to our previous implementation.²³ Once the rates for all possible events are determined at a given simulation time t , an event i is chosen with probability $\Gamma_i/\Sigma\Gamma_k$ and executed at time $t - \ln u/\Sigma\Gamma_k$, where $u \in (0, 1]$. After the event is executed, the rate database is updated, and a new event is chosen based on the new rates. We use a method similar to the next reaction method²⁴ for rate selection, which scales as $\log(N_T)$ for each step, where N_T is the total number of possible events. There are a maximum of six possible events per particle in the algorithm: up to four move events, an aggregation event, and a particle-switching event, which is defined in Sec. III B.

A. Particle blocking in an aggregating system—Extensions to the pass-forward algorithm

Particle blocking introduces artifacts in the dynamics when convection is present; this phenomenon has been addressed in detail in a previous publication.²³ Briefly, particles immediately upstream from other particles cannot move in the direction of flow due to site exclusion and therefore have a convective rate of 0. In Ref. 23, it was found that by passing forward the rates of blocked particles in a connected chain to the first nonblocked particle, the convective rates of all particles are corrected in an averaged sense; this method was termed the pass-forward algorithm, or PFA. In our previous implementation of the PFA (without aggregation), monomers

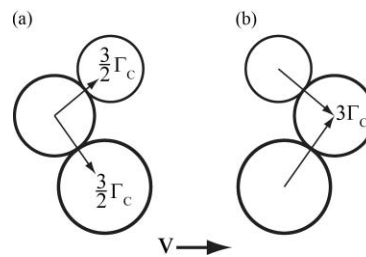


FIG. 2. Rate passing scheme. (a) A particle can be blocked from moving in the direction of flow by two (or more) particles. The convective rate of the blocked particle is passed forward in equal parts to each blocking particle. Assuming each particle has the same initial convective rate, Γ_C , the new convective rates for the blocking particles are $\frac{3}{2}\Gamma_C$. (b) Conversely, a single particle can block two (or more) particles in the direction of flow. The convective rate of each blocked particle is passed forward to the blocking particle. Assuming each particle has the same initial convective rate, Γ_C , the new convective rate for the blocking particle is $3\Gamma_C$.

were assigned to single lattice sites, i.e., $\alpha = 1$ for all time. With aggregation present, particles can occupy multiple lattice sites and generally, $\alpha > 1$. In this case, a given particle can be blocked by multiple other particles. The reverse situation is also possible, in which one particle directly blocks several others; examples are shown in Fig. 2. The PFA is readily applicable to any arbitrary particle connectivity. As shown in Fig. 2, the convective rates are passed forward (in the direction of flow) to the blocking particles based on the local connectivity. For example, Fig. 2(a) shows the situation when two particles block a third; here, the convective rate of the blocked particle is partitioned evenly among the two blocking particles. Conversely, when one particle blocks two others, the sum of the blocked particle convective rates is passed forward to the blocking particle, as shown in Fig. 2(b).

III. RESULTS AND DISCUSSION

First, we employ a series of calculations to validate the LKMC model against well-established PBE solutions. We then examine examples that demonstrate the flexibility of the LKMC approach by considering particle aggregation in more complex flows, and make connections to the specific case of platelet clustering. In all cases, we consider two-dimensional geometries.

A. Ideal ($\varepsilon = 1$) aggregation in a two-dimensional, constant shear flow

We consider a two-dimensional representation of a cone-and-plate geometry into which circular particles of uniform radius R_0 are initially placed with concentration C_0 . The initial volume fraction is $\phi = C_0\pi R_0^2$. The computational domain is represented by a rectangular box of size $L_x = 40$, $L_y = 0.3$. A shear rate G is applied in the y dimension so that the velocity profile within the domain is $v_x(y) = Gy$. Periodic boundaries are applied in the direction of flow and no flux boundaries are imposed perpendicular to the direction of flow. The particles in the fluid are assumed to move along rectilinear paths until collision, i.e., no hydrodynamic or other particle interactions are explicitly modeled here.

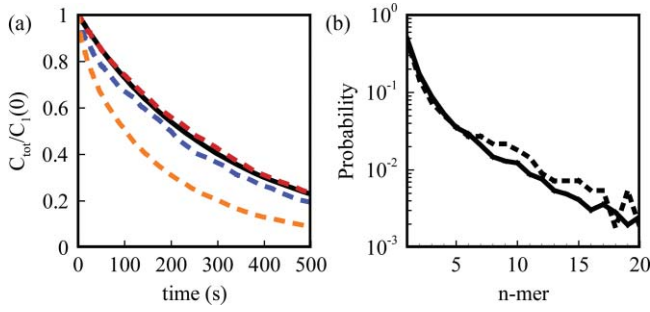


FIG. 3. Ideal aggregation of particles at constant shear for $\phi = 0.005$, where Φ is the area fraction, $G = 1s^{-1}$, $\varepsilon = 1$, $L_x = 40$, and $L_y = 0.3$. (a) Evolution of total particle concentration, $C_{\text{tot}} = \sum C_i$, normalized by the initial monomer concentration, $C_1(0)$. Black: PBE, orange: LKMC $\alpha = 1$, blue: LKMC $\alpha = 5$, red: LKMC $\alpha = 15$. (b) Particle distribution at $t = 500$ s for PBE (solid line) and LKMC (dotted line) with $\alpha = 15$.

The population balance equation for aggregates of size i is given by considering collisions that create and destroy particles of size i :

$$\frac{dC_i}{dt} = \frac{1}{2} \sum_{j=1}^{i-1} \varepsilon k_{j,i-j} C_j C_{i-j} - \sum_{j=1}^{\infty} \varepsilon k_{i,j} C_i C_j, \quad (6)$$

where $\varepsilon k_{ij} C_i C_j$ is the rate of aggregation between clusters of size i (an “ i -mer”) and clusters of size j to form clusters of size $i + j$, C_i and C_j are the concentration of i -mers and j -mers, respectively, and k_{ij} is the collision kernel that depends on the fluid flow. Note that the collision efficiency ε can include hydrodynamic interactions and other interparticle interactions such as receptor capture efficiency between individual cells.^{7,8,25,26} For the case of two-dimensional aggregation of circular particles in constant shear, the collision kernel is given by (see the Appendix for derivation)

$$k_{ij} = G (R_i + R_j)^2. \quad (7)$$

The PBE has no known analytic solution even for this simple kernel, but several methods exist for numerical solution.^{27,28} We use a stochastic numerical solution approach²⁹ based on the Gillespie method for chemical kinetics,³⁰ which is essentially a mean-field version of the LKMC algorithm employed here.

The concentration of particles in a constant-shearing fluid as a function of time is shown in Fig. 3(a) for both the LKMC and PBE methods when $\varepsilon = 1$ ($\Gamma_{\text{agg}} = \infty$). The decreasing aggregation rate results from the decreasing particle concentration as the aggregation process continues. In fact, as shown in Eq. (6), the aggregation rate is expected to scale as the square of the particle concentration. The agreement between the LKMC results and the PBE solution is strongly influenced by the resolution of the lattice. For coarse lattices, particles tend to aggregate too rapidly, an error that arises from the diffusive error described in Sec. II, which creates additional collisions due to diffusive motion in the direction of flow. This error decreases as the lattice spacing decreases, and for values of α greater than approximately 10, the LKMC results match the PBE for all simulated time. A more detailed comparison between the two methods at a specific time is shown in Fig. 3(b), where individual components of the overall size

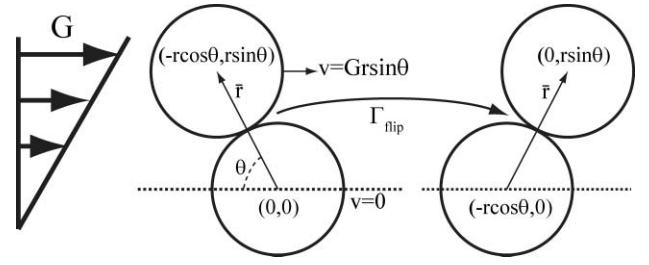


FIG. 4. Particle switching causes nonideal collisions in LKMC. The vector that points from the center of the reference sphere to the center of the colliding sphere is \vec{r} , which makes an angle θ to the direction of flow and has a magnitude of $r = R_i + R_j$, where i and j are the reference sphere and colliding sphere. At a local shear rate G , the colliding particle has a relative velocity of $G r \sin\theta$. The colliding particle moves $r \cos\theta$ and the reference particle moves $-r \cos\theta$ in the direction of flow.

distribution are shown. For $\alpha = 15$ at $t = 500$ s, the agreement is quantitative within the spread of the LKMC results.

B. Nonideal ($\varepsilon < 1$) aggregation in a two-dimensional, constant shear flow

The lack of explicit hydrodynamic interparticle interactions in the present LKMC algorithm can create artifacts in the nonideal collision case. Consider the situation where a faster-moving particle approaches a slower-moving one and becomes blocked. In the ideal collision case, instantaneous aggregation results and a new, single particle is created. In the nonideal case (finite Γ_{agg}), however, the blocking cannot be resolved until the particles aggregate. In other words, an aggregation event will take place for every collision even when Γ_{agg} is very small, because there is no mechanism for the colliding particles to disentangle following the collision. In reality, lubrication forces allow particles to slide around each other over a finite time interval.

This difficulty is resolved by introducing an additional event, namely the switching of coordinates in the direction of flow of a pair of particles after some time, as shown in Fig. 4. Consider two nearest-neighbor particles, i and j , colliding at an angle θ with respect to the direction of flow (see Fig. 4). The interaction time for this event is assumed to be $\Delta t = (2\Delta x/\Delta v)$, where Δx is the center-to-center separation distance in the direction of flow, and Δv is the velocity difference between the two particles. As shown in Fig. 4, $\Delta x = (R_i + R_j) \cos\theta$ and $\Delta v = G(x, y) (R_i + R_j) \sin\theta$. Combining these expressions provides a time scale for switching as a function of the contact angle,

$$\Delta t = \frac{2}{G} \cot\theta. \quad (8)$$

The corresponding rate expression for pair switching is given by

$$\Gamma_{\text{flip}} = \frac{G}{2} \tan\theta. \quad (9)$$

The pair-interaction time (or equivalently the switching rate) in this model does not depend on the radii of the interacting particles, a result that is consistent with experimentally measured particle interaction times.³¹

We now make quantitative connections between the collision efficiency parameter, the switching rate, Γ_{flip} , and the aggregation rate, Γ_{agg} . Over the contact time interval, and for a given (constant) aggregation rate, the probability that two particles have not aggregated is exponentially distributed. Therefore, the probability that the particles have aggregated with a specific angle of contact is

$$P(\theta) = 1 - \exp(-\Gamma_{\text{agg}} \Delta t) = 1 - \exp\left(-2 \frac{\Gamma_{\text{agg}}}{G} \cot \theta\right). \quad (10)$$

The collision efficiency ε is the probability that any collision between two particles will produce a successful aggregation event. The collision efficiency within a LKMC simulation is generally given by

$$\varepsilon = \frac{\int_0^{\pi/2} J(\theta) P(\theta) d\theta}{\int_0^{\pi/2} J(\theta) d\theta}, \quad (11)$$

where $J(\theta)$ is the flux of particles arriving at a reference particle position with collision angle θ . In the case of rectilinear particle trajectories with locally constant shear, the arrival flux is given by

$$J(\theta) = C_j G (R_i + R_j) \sin \theta. \quad (12)$$

Note that the arrival flux is nonuniform and increases with increasing contact angle. Inserting Eq. (12) into Eq. (11) provides an expression for the average sticking probability based on LKMC parameters,

$$\varepsilon = 1 - \int_0^{\pi/2} \sin \theta \exp\left(-2 \frac{\Gamma_{\text{agg}}}{G} \cot \theta\right) d\theta. \quad (13)$$

The collision efficiency is therefore explicitly dependent on the dimensionless ratio of the aggregation rate to the shear rate, (Γ_{agg}/G) .

The integral expression in Eq. (13) was evaluated numerically for $10^{-3} < (\Gamma_{\text{agg}}/G) < 10^3$ as shown in Fig. 5(a). When the aggregation rate is large relative to the shear rate, the ideal aggregation limit is obtained and $\varepsilon \sim 1$. As the aggregation becomes small relative to the shear rate,

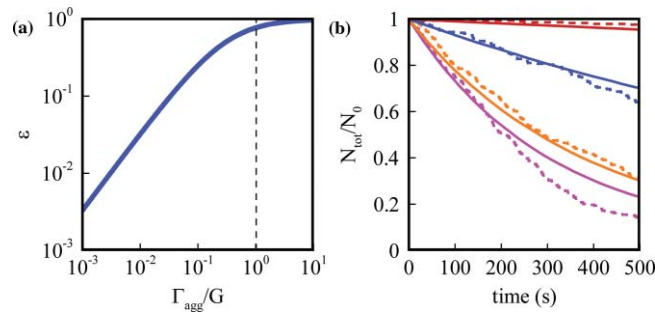


FIG. 5. Nonideal collisions at constant shear. (a) Numerical integration of collision efficiency varying with the ratio of the aggregation rate to the shear rate [Eq. (13)]. (b) Comparison between LKMC (dashed lines) for various ratios of aggregation to shear rate [0.01 (red), 0.1 (blue), 1 (orange), and 100 (purple)] and PBE (solid lines) with corresponding collision efficiency determined from numerical integral from panel (a). $G = 1 \text{ s}^{-1}$, $\phi = 0.005$, $\alpha = 10$, $L_x = 20$, $L_y = 1$, and $R_0 = 0.001$ for all LKMC simulations.

$\varepsilon \rightarrow 0$. The crossover between ideal collisions ($\varepsilon = 1$) and noninteracting collisions appears naturally at $(\Gamma_{\text{agg}}/G) \approx 1$, confirming the relevance of this ratio in dictating the overall collision efficiency. Equation (13) and Fig. 5(a) provide the correspondence between the spatially resolved particle interactions, through the rate of aggregation and the interaction time, and the spatially averaged collision efficiency in the PBE. Since the interaction time depends only on the local flow characteristics in this model, only one free parameter, Γ_{agg} , needs to be specified in LKMC. Choice of this parameter for a physical system is discussed in Sec. III C.

LKMC simulations of aggregation in the periodic, two-dimensional constant-shearing flow were performed for $10^{-2} < (\Gamma_{\text{agg}}/G) < 10^2$ and $G = 1 \text{ s}^{-1}$. The temporal evolution of the total number of clusters for the different cases is compared to the corresponding PBE simulations in Fig. 5(b). In each PBE case, the corresponding value of ε was obtained from Fig. 5(a), and agreement between the two simulation approaches is observed over 4 orders of magnitude in the parameter (Γ_{agg}/G) . Note that for coarse size distributions, the total number of clusters is small, and the corresponding statistical fluctuations in the LKMC result become larger.

C. Platelet aggregation in tubular channels

Here, we demonstrate the ability of the contact time model to reproduce the behavior of a physical system with hydrodynamic interactions and cellular bonding. Bell *et al.*⁴ have measured size distributions of adenosine diphosphate (ADP)-stimulated platelet aggregates at the outlet of a tube at four average shear rates: 41.9, 168, 335, and 1000 s^{-1} . By assuming a linear velocity profile at the average shear rate of the tube, it was possible to extract an effective collision efficiency for platelets. Overall, the collision efficiency was found to decrease with increasing shear rate, a result that is qualitatively consistent with the particle interaction model presented in Sec. III B.

We make an explicit connection to the LKMC contact time by finding the single aggregation rate parameter that leads to the best match to the inferred collision efficiency at each shear rate in Ref. 4. The best fit value of the aggregation rate is found to be $\Gamma_{\text{agg}} = 0.683 \text{ s}^{-1}$. As shown in Fig. 6, the contact time model used in the LKMC model provides a good quantitative description of the shear-rate dependence on the collision efficiency for platelets. The dotted lines represent $\pm 50\%$ of the regressed rate of aggregation, which captures some of the uncertainty due to the approximations used to calculate the collision efficiency in Ref. 4. The regressed aggregation rate can be qualitatively interpreted in terms of the time required to form bonds that are strong enough to hold platelets together. The value of $\Gamma_{\text{agg}} = 0.683 \text{ s}^{-1}$ is a net aggregation rate that characterizes the result of fast (but unstable) GPIIb-von Willebrand bonds and slower (but stable) glycoprotein $\alpha_{2b}\beta_3$ -fibrinogen bonds. Multiple bonds between $\alpha_{2b}\beta_3$ on one platelet and bound fibrinogen on another platelet are required for stable aggregation, and $\Gamma_{\text{agg}} = 0.683 \text{ s}^{-1}$ is consistent with $O(1\text{s})$ time for the multiple high affinity $\alpha_{2b}\beta_3$ -fibrinogen complex to form since $O(0.1\text{s})$ time is needed for a single bond to form.³²

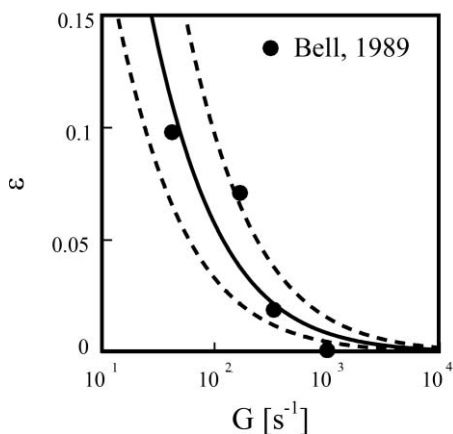


FIG. 6. Comparison of particle interaction model with experimentally determined collision efficiencies for ADP stimulated platelet aggregation. Circles show data from Ref. 4. Solid line is the particle interaction model with an aggregation rate of 0.683 s^{-1} . Dotted lines are the particle interaction model with an aggregation rate of $0.683 \pm 50\%$.

D. Aggregation in nonperiodic, open systems

We now consider the more general case of open systems, in which the aggregation process takes place along a domain of finite length under specified inlet conditions. We consider four types of flow: plug flow, constant-shear flow, parabolic parallel-plate flow, and a more complex situation with baffles. In the following simulations, the inlet condition is a fixed particle volume fraction of monomers with a uniform radius distribution, R_0 . This inlet condition is implemented by defining a new event in the LKMC simulation that inserts a particle into the domain such that the center of mass is R_0/h lattice units from the boundary, which allows for the insertion of the entire particle onto the lattice. The rate for inserting a particle with center of mass located at a specific lattice site i is proportional to the total flux of fluid through that lattice site, $v_i h$, and the concentration of monomer particles in the inlet, C_0 , or

$$\Gamma_{\text{inlet}}(i) = v_i h C_0. \quad (14)$$

Only the overall inlet rate, $\Sigma \Gamma_{\text{inlet}}(j)$, where the summation is only over valid inlet sites, is used as an event in LKMC to determine when a new particle is inserted into the domain. After that event is chosen to occur, the particle's cen-

ter of mass is placed at a specific lattice site i with probability $\Gamma_{\text{inlet}}(i)/\Sigma \Gamma_{\text{inlet}}(j)$. If this causes particle-particle overlap, this site is rejected and a new site is chosen until site exclusion is satisfied.

In the following examples, a finite, rectangular domain with dimensions $L_x = 20$, $L_y = 1$ was employed. A uniformly distributed square lattice with $h = 0.001$ was used in all cases. We first compare the behavior of aggregation in two flows: constant shear and parabolic. In the constant-shear case, the prescribed velocity profile is given by $v_x(y) = 2 \times 10^5 y$, while the parabolic velocity profile is $v_x(y) = 3 \times 10^5 (1 - y^2)$. In the latter case, the y origin is defined at the centerline of the domain. The total flow rate in both cases is the same. Steady-state quantities, averaged over sufficiently long time intervals, are measured for open systems whereas time-dependent quantities were measured in Figs. 3 and 5. In Fig. 7, the aggregation rates at steady state are compared for both flows. As seen by Eqs. (6) and (7), the aggregation rates scale as $\sim GC^2$. Note that although the shear rate is constant across the height of the domain in the first case [Fig. 7(a)], the aggregation rate is not. The reason for this apparent anomaly is a direct consequence of the variation in residence time across the height of the channel. Thus, more time for particle aggregation is available in the slower-moving streamlines and the aggregation rate decreases more rapidly with distance along the length of the channel. The large values for aggregation rate are a direct result of the large shear rate. In the parabolic flow case, the y locations with the highest aggregation rates along the channel occur near, but not at, the plate surfaces. These regions present an optimal balance between high shear rate and relatively low residence time. The corresponding average particle sizes at steady state as well as a representative snapshot are shown in Fig. 8 for both cases. As expected, regions that exhibit the longest residence time show the largest particles—in both cases, this is the region of the flow adjacent to the channel walls. Note that the average particle size is expected to correlate with the product of the aggregation rate and the residence time integrated along the length of the channel.

The mixing-cup averaged size distributions of particles exiting the two channels are shown in Fig. 9, along with results obtained from an idealized plug-flow case. Although the total flow rate is the same in all three cases, the parabolic flow example leads to the largest particles on average. The reason

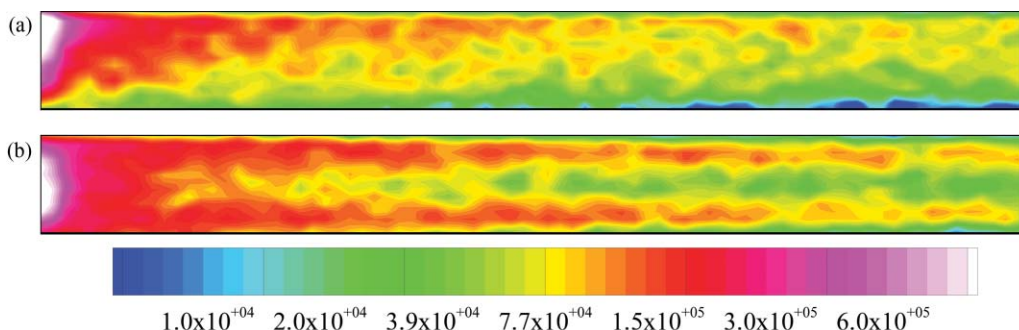


FIG. 7. Comparison of aggregation rates for constant shear rate and parabolic flow in an open system. Colorbar is in units of aggregation events per unit area time. Flow is from left to right with dimensions $L_x = 20$ and $L_y = 1$. The aspect ratio of each panel is 10:1 for readability. $\alpha = 10$, $h = 0.001$, $\phi = 0.01$, and $R_0 = 0.01$. (a) Constant shear rate with an average velocity of $2E5$. (b) Parabolic flow with an average velocity of $2E5$.

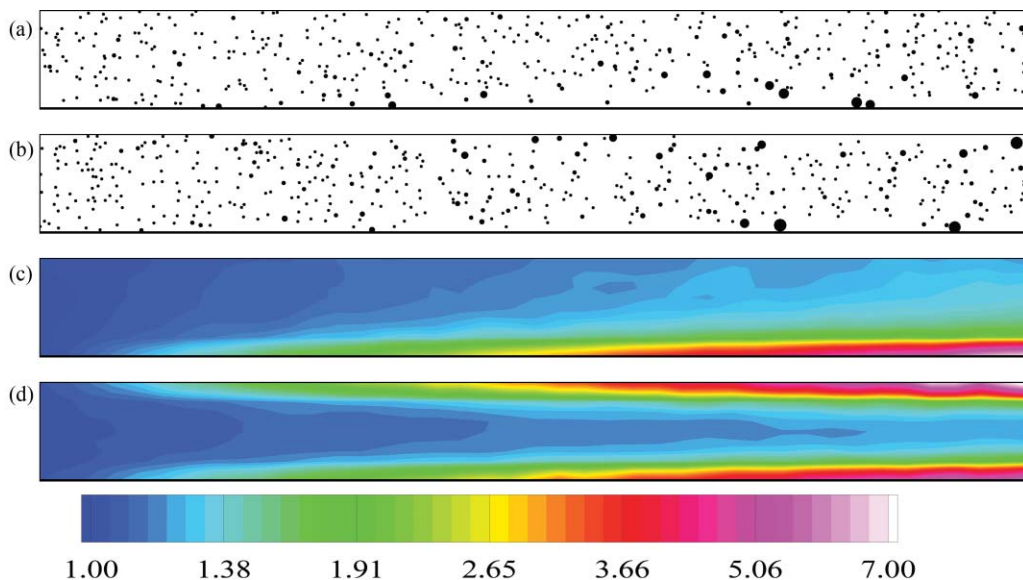


FIG. 8. Comparison of particle size for constant shear rate and parabolic flow in an open system. Flow is from left to right with dimensions $L_x = 20$ and $L_y = 1$. The aspect ratio of each panel is 10:1 for readability: $\alpha = 10$, $h = 0.001$, $\phi = 0.01$, and $R_0 = 0.01$. (a,c) Constant shear rate with an average velocity of $2E5$. (b, d) Parabolic flow with an average velocity of $2E5$. (a-b) Snapshot of particles during simulation. Radii of particles enhanced by a factor of 3. (c-d) Color bar represents average particle size relative to the monomer size: $(R/R_0)^2$.

for this can be understood mathematically by considering an approximate solution to the PBE in which all particles are assumed to be the same size. The PBE system is reduced to a single differential equation of the form⁶

$$\frac{dC_\infty}{dt} = -\frac{2\phi}{\pi} GC_\infty, \quad (15)$$

where C_∞ is the concentration of the single-particle size in the system and ϕ is the area fraction of particles in 2D. Integrating along a particular streamline in unidirectional flow³³ gives

$$\frac{C_\infty}{C_\infty(0)} = \exp\left(-\frac{2\Phi}{\pi} G\left(\frac{L}{v}\right)\right), \quad (16)$$

where L is the length and v is the velocity along the streamline. The mixing-cup averaged concentration of particles

exiting the channel is then given by the expression

$$\frac{\bar{C}_\infty}{C_\infty(0)} = \frac{\int v \frac{C_\infty(y)}{C_\infty(0)} dy}{\int v dy}. \quad (17)$$

Numerical solution of Eq. (17) demonstrates that, for short channels, more aggregation takes place in parabolic flow due to the low-velocity regions near the walls, consistent with the results in Fig. 9. However, as the channel length increases, the averaged aggregation extent becomes greater in the constant-shear-rate case due to regions of low shear near the center of the channel in parabolic flow. The crossover occurs at a length-to-height ratio of 65.

We conclude this section by noting that the plug-flow channel ($v_x = 2 \times 10^5$) also leads to measurable aggregation (Fig. 10), even though the aggregation kernel should be zero. Here, all aggregation events are driven by the algorithmic

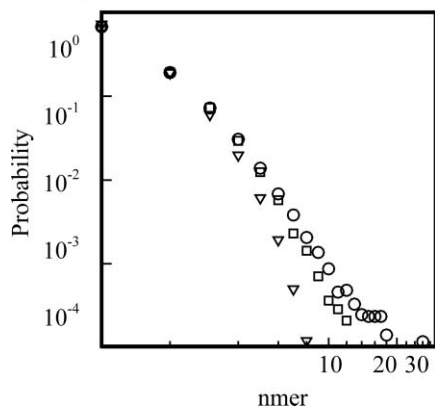


FIG. 9. Outlet distribution at steady state for open systems. Triangles—plug flow. Squares—constant shear rate. Circles—parabolic flow. Flow is from left to right with dimensions $L_x = 20$ and $L_y = 1$. $\alpha = 10$, $h = 0.001$, $\phi = 0.01$, and $R_0 = 0.01$, average velocity of $2E5$.

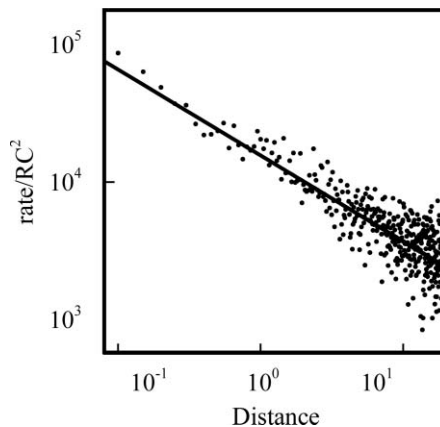


FIG. 10. Comparison of 1D Brownian aggregation [kernel in Eq. (B2)] (line) to plug flow LKMC simulation (symbols). The radius of particles in LKMC is taken as the average particle radius at that position. Dimensions of $L_x = 20$ and $L_y = 1$. $\alpha = 10$, $h = 0.001$, $\phi = 0.01$, $R_0 = 0.01$, and $v = 2 \times 10^5$.

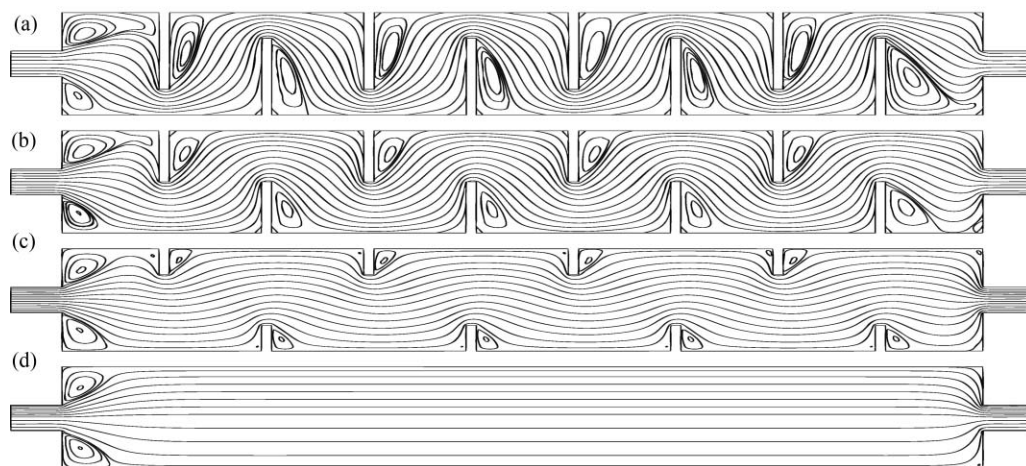


FIG. 11. Streamlines for baffle reactors with flow from left to right. Overall dimensions of reactor are $L_x = 20$ and $L_y = 2$. Inlet and outlet have length 1 and width 0.5. Baffles are 0.2 units thick and (a) 1.5 units, (b) 1 unit, (c) 0.5 units, and (d) 0 units long. $\alpha = 10$, $h = 0.00133$, $\phi = 0.02$, and $R_0 = 0.00133$.

diffusion in the LKMC simulation. It is possible to demonstrate that the aggregation rate obtained in the plug-flow case can be quantitatively reproduced by solving the PBE using a Brownian motion kernel (see the Appendix). The amount of artificial aggregation is small, however, and particle size increases slowly along the channel relative to the real, shear-driven process. We note once again that this artificial source of aggregation can be reduced arbitrarily by increasing the grid resolution relative to the monomer size.

E. Aggregation in complex flows: Parallel plate reactor with baffles

The validated LKMC model was used to investigate particle aggregation in a more complex flow produced in a rectangular channel containing baffles to introduce additional fluid shear. Our choice of this type of flow geometry is motivated by stenotic or valvular flows, which present regions of

high shear (squeeze flow) and regions of high residence time (standing vortices). Such geometries cannot be considered in a mean-field PBE framework, necessitating the use of a spatially resolved approach. The LKMC simulation domain considered here includes a total of eight baffles that are equally spaced and originate from alternating channel walls, as shown in Fig. 11. Four cases are considered in which the baffle height is varied from zero to 0.75 of the channel width. The resulting flow streamlines for each case are shown in Fig. 11. The fluid is incompressible, and the average normal velocity in the inlet is 20 ($Re = 10$). The velocity field for each geometry was determined by a finite-element solution of the Navier-Stokes equation (COMSOL MultiphysicsTM, Burlington, MA).

The particle aggregation rates are shown for all four cases in Fig. 12. The effect of the baffles is generally to locally increase the shear rate and therefore the aggregation rate, an effect that increases with increasing baffle height. Note that as the particles coarsen, the aggregation rate decreases down

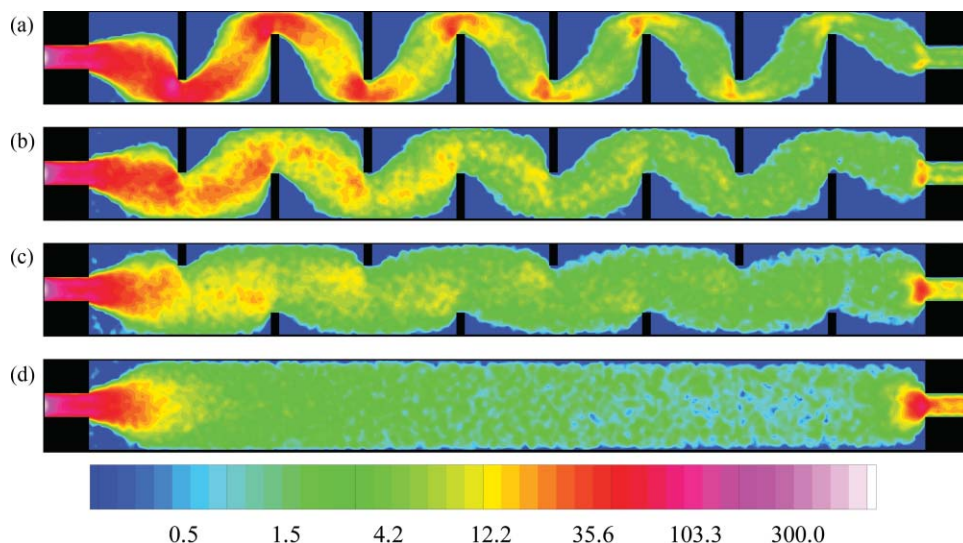


FIG. 12. Aggregation rate at steady state in baffle reactors from Fig. 11. Color bar is in units of aggregation events per unit area time. Overall dimensions of the reactor are $L_x = 20$ and $L_y = 2$. Inlet and outlet have length 1 and width 0.5. Baffles are 0.2 units thick and (a) 1.5 units, (b) 1 unit, (c) 0.5 units, and (d) 0 units long. $\alpha = 10$, $h = 0.00133$, $\phi = 0.02$, and $R_0 = 0.00133$.

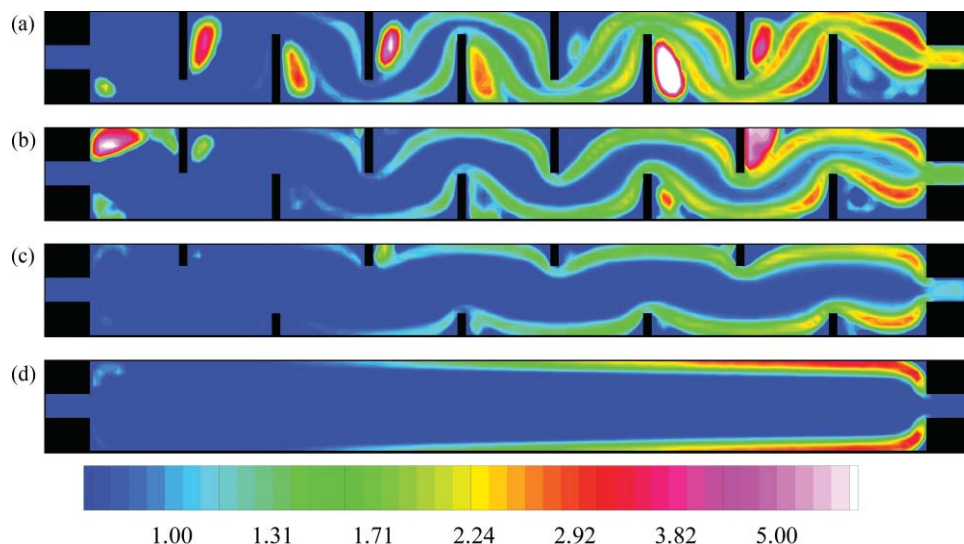


FIG. 13. Average dimensionless particle size at steady state in baffle reactors from Fig. 11. Color bar represents average particle size relative to the monomer size: $(R/R_0)^2$. Overall dimensions of reactor are $L_x = 20$ and $L_y = 2$. Inlet and outlet have length 1 and width 0.5. Baffles are 0.2 units thick and (a) 1.5 units, (b) 1 unit, (c) 0.5 units, and (d) 0 units long. $\alpha = 10$, $h = 0.00133$, $\phi = 0.02$, and $R_0 = 0.00133$.

the channel due to lower particle concentration. In the recirculation regions adjacent to each baffle, the aggregation rate is very low corresponding to the very low shear rate there. The corresponding average particle-size distribution for each case is shown in Fig. 13. Most notably, extremely large particles are found in the recirculation regions where the residence time is very long, leading to a broad size distribution at the reactor exit. This often undesirable effect increases with increasing baffle height, demonstrating how the present simulation tool could be used to optimize reactor geometries in the presence of competing objectives.

IV. CONCLUSIONS

A new approach based on the lattice kinetic Monte Carlo (LKMC) method is presented for simulating particle aggregation in the presence of complex fluid flow. In this work, we build on a recently developed method to include convection within LKMC simulations. LKMC is a versatile and computationally attractive technique for simulation of the spatiotemporal evolution of a collection of particles. For example, an open-system simulation that tracked on the order of 100 000 particles and aggregates of up to 80-mers required approximately 6 h on a single CPU. However, essentially no work has been applied toward the consideration of convection (e.g., flow) as a driving force for particle motion. In previous work, we demonstrated an algorithm that resolves unexpected numerical difficulties associated with the sequential single-particle move nature of the LKMC technique when drift is present. In the present paper, we extended this work to include explicit particle aggregation, thereby allowing us to consider a far broader range of problems than has been possible with LKMC.

A key aspect of the aggregation physics embodied in the present algorithm is a contact time model that was developed to account for the finite time that particles in close proximity have to establish an aggregated state. The need for an explicit

contact time model stems from the lack of hydrodynamic interactions within the present implementation of the LKMC algorithm. The contact time model accounts for the local shear rate and particle-particle contact angle to generate an expression for the probability of particle-particle binding in terms of the LKMC parameters that is compatible with the sticking coefficient parameter commonly employed in mean-field models and experimental measurements. We analyzed the contact time model further in the context of platelet aggregation using regression to experimentally inferred sticking coefficients in a tubular microchannel. Here, we find that it is possible to make a quantitative connection between the LKMC aggregation rate parameter and “bond” formation during platelet-platelet sticking. Specifically, a single extracted aggregation rate is able to adequately describe an experimentally inferred platelet collision efficiency across a large range of averaged shear rates within tubular flow. Moreover, the inferred aggregation rate is physiologically reasonable, which provides further evidence for the utility of the computationally efficient approach taken in this work.

The LKMC model presented in this paper was validated using a series of simple examples that can be described with a population balance equation formulation. Although the LKMC simulations were fully able to capture the spatiotemporal evolution in all tested cases, we find that the lattice spacing relative to the particle size is an important parameter in setting the accuracy of the method. In general, coarser grids lead to an increase in numerical diffusion, which alters the physics of the aggregation process. The LKMC model was then applied to flow examples that are well beyond the scope of PBE-based approaches. In particular, we considered a baffled parallel-plate geometry with variable baffle geometry that produces a highly heterogeneous shear-rate distribution within the domain. It was demonstrated that the LKMC approach is easily able to address such complex situations and generate an explicit particle-size distribution throughout the geometry.

ACKNOWLEDGMENTS

This work was supported by NIH Grant No. R01-H656621 (S.L.D.), NIH Grant No. R33-HL-87317 (S.L.D.), and NIH Grant No. R01-HL-103419 (S.L.D.).

APPENDIX A: TWO-DIMENSIONAL AGGREGATION KERNEL IN SHEARING FLOW

The flux of particles of radius R_j at a concentration, C_j , to reference particles of radius R_i in a constant shearing flow is given by

$$\begin{aligned} J_{ij} &= 2 \int_0^{R_i+R_j} C_j C_i v_{ij} dr \\ &= 2C_j C_i \int_0^{R_i+R_j} G r dr \\ &= C_j C_i G (R_i + R_j)^2 \end{aligned} \quad (\text{A1})$$

where v_{ij} is the relative particle velocity. With the relation $J_{ij} = k_{ij} C_i C_j$, the result in Eq. (7) is obtained.

APPENDIX B: ONE-DIMENSIONAL BROWNIAN AGGREGATION KERNEL

To derive the time-dependent aggregation kernel, consider a set of particles at initial concentration C_0 diffusing in one dimension. Here, we consider the motion of the particles with respect to a reference particle in the positive x direction. The boundary condition at the surface of the reference particle is $C(x, t) = 0$ for ideal collisions. To compare the results to the pseudo-steady aggregation kernel, we assume that the far-field concentration does not change, i.e., $C(\infty, t) = C_0$. The concentration profile around the reference sphere is given by the diffusion equation $(\partial C / \partial t) = 2D(\partial^2 C / \partial x^2)$, where the factor of 2 comes from fixing the reference particle. The solution for this PDE collapses onto a single solution with respect to a penetration length that grows as the square root of time $C(x, t) = C_0 \text{erf}(-\frac{x}{g(t)})$, $g(t) = 2(2Dt)^{1/2}$. The flux of particles to the reference particle surface at $x = 0$ is

$$\begin{aligned} \text{Flux}_+ &= -2R_{\text{collision}} D \left. \frac{\partial C}{\partial x} \right|_{x=0} \\ &= 2(R_i + R_j) \left(\frac{2D}{\pi t} \right)^{1/2} C_0, \end{aligned} \quad (\text{B1})$$

where $\left. \frac{\partial C}{\partial x} \right|_{x=0} = C_0 \left(\frac{2}{\pi Dt} \right)^{1/2}$, $R_{\text{collision}} = R_i + R_j$, and the subscript + indicates flux of particles from the pos-

itive x direction. The total flux per unit area is $\text{Flux}_{\text{total}} = \frac{1}{2}(|\text{Flux}_+| + |\text{Flux}_-|)C_0 = 2(R_i + R_j)(2D/\pi t)^{1/2}C_0^2$, where the factor of 1/2 arises from double counting collisions and the absolute value of the flux from the positive and negative directions are equal. The kernel is

$$k = 2(R_i + R_j) \left(\frac{2D}{\pi t} \right)^{1/2}. \quad (\text{B2})$$

- ¹E. Brunet, G. Degré, F. Okkels, and P. Tabeling, *J. Colloid Interface Sci.* **282**, 58 (2005).
- ²C. Xiong and S. K. Friedlander, *Proc. Natl. Acad. Sci. USA* **98**, 11851 (2001).
- ³A. D. Taylor, S. Neelamegham, J. D. Hellums, C. W. Smith, and S. I. Simon, *Biophys. J.* **71**, 3488 (1996).
- ⁴D. Bell, S. Spain, and H. L. Goldsmith, *Biophys. J.* **56**, 817 (1989).
- ⁵S. Neelamegham, A. D. Taylor, J. D. Hellums, M. Dembo, C. W. Smith, and S. I. Simon, *Biophys. J.* **72**, 1527 (1997).
- ⁶S. K. Friedlander, *Smoke, Dust, and Haze: Fundamentals of Aerosol Dynamics*, 2nd ed. (Oxford University Press, New York, 2000).
- ⁷T. G. M. van De Van and S. G. Mason, *Colloid Polymer Sci.* **255**, 468 (1977).
- ⁸P. Adler, *J. Colloid Interface Sci.* **83**, 106 (1981).
- ⁹H. H. Hu, N. A. Patankar, and M. Y. Zhu, *J. Comput. Phys.* **169**, 427 (2001).
- ¹⁰A. J. C. Ladd and R. Verberg, *J. Stat. Phys.* **104**, 1191 (2001).
- ¹¹P. J. Hoogerbrugge and J. M. V. A. Koelman, *Europhys. Lett.* **19**, 155 (1992).
- ¹²J. S. Marshall, *J. Aerosol Sci.* **38**, 333 (2007).
- ¹³J. A. Mousel and J. S. Marshall, *Microfluidics Nanofluidics* **8**, 171 (2009).
- ¹⁴K. Leiderman and A. L. Fogelson, *Math. Med. Biol.* (published online).
- ¹⁵Z. Xu, J. Lioi, J. Mu, M. M. Kamocka, X. Liu, D. Z. Chen, E. D. Rosen, and M. Alber, *Biophys. J.* **98**, 1723 (2010).
- ¹⁶Z. Xu, N. Chen, M. M. Kamocka, E. D. Rosen, and M. Alber, *J. Royal Soc. Interface* **5**, 705 (2008).
- ¹⁷T. P. Schulze, *Phys. Rev. E* **78**, 020601 (2008).
- ¹⁸A. Levi, C. Levi, and M. Kotrla, *J. Phys.: Condens. Matter* **9**, 299 (1997).
- ¹⁹J. Dai, J. M. Kanter, S. S. Kapur, W. D. Seider, and T. Sinno, *Phys. Rev. B* **72**, 134102 (2005).
- ²⁰J. Dai, W. D. Seider, and T. Sinno, *Mol. Sim.* **33**, 733 (2007).
- ²¹A. Chatterjee, D. G. Vlachos, and M. A. Katsoulakis, *J. Chem. Phys.* **121**, 11420 (2004).
- ²²J. Dai, W. D. Seider, and T. Sinno, *J. Chem. Phys.* **128**, 194705 (2008).
- ²³M. H. Flamm, S. L. Diamond, and T. Sinno, *J. Chem. Phys.* **130**, 094904 (2009).
- ²⁴M. A. Gibson and J. Bruck, *J. Phys. Chem. A* **104**, 1876 (2000).
- ²⁵P. Tandon and S. L. Diamond, *Biophys. J.* **73**, 2819 (1997).
- ²⁶P. Tandon and S. L. Diamond, *Biophys. J.* **75**, 3163 (1998).
- ²⁷D. Ramkrishna and S. Kumar, *Chem. Eng. Sci.* **51**, 1311 (1996).
- ²⁸M. Smith and T. Matsoukas, *Chem. Eng. Sci.* **53**, 1777 (1998).
- ²⁹I. J. Laurenzi and S. L. Diamond, *Phys. Rev. E* **67**, 051103 (2003).
- ³⁰D. T. Gillespie, *J. Comput. Phys.* **22**, 403 (1976).
- ³¹R. S. J. Manley and S. G. Mason, *J. Colloid Sci.* **7**, 354 (1952).
- ³²R. I. Litvinov, J. S. Bennett, J. W. Weisel, and H. Shuman, *Biophys. J.* **89**, 2824 (2005).
- ³³J. Gregory, *Chem. Eng. Sci.* **36**, 1789 (1981).